Monitoring Vital Signs and Postures During Sleep Using WiFi Signals

Jian Liu, Yingying Chen, *Senior Member, IEEE*, Yan Wang, *Member, IEEE*, Xu Chen, Jerry Cheng, *Member, IEEE*, and Jie Yang, *Member, IEEE*

***Abstract*—Tracking human sleeping postures and vital signs of breathing and heart rates during sleep is important as it can help to assess the general physical health of a person and provide useful clues for diagnosing possible diseases. Traditional approaches (e.g., polysomnography) are limited to clinic usage. Recent radio frequency-based approaches require specialized devices or dedicated wireless sensors and are only able to track breathing rate. In this paper, we propose to track the vital signs of both breathing rate and heart rate during sleep by using off-the-shelf WiFi without any wearable or dedicated devices. Our system reuses existing WiFi network and exploits the fine-grained channel information to capture the minute movements caused by breathing and heart beats. Our system thus has the potential to be widely deployed and perform continuous long-term monitoring. The developed algorithm makes use of the channel information in both time and frequency domain to estimate breathing and heart rates, and it works well when either individual or two persons are in bed. Our extensive experiments demonstrate that our system can accurately capture vital signs during sleep under realistic settings, and achieve comparable or even better performance comparing to traditional and existing approaches, which is a strong indication of providing noninvasive, continuous fine-grained vital signs monitoring without any additional cost.**

***Index Terms*—Channel state information (CSI), sleep monitoring, vital signs, WiFi.**

I. Introduction

VITAL signs, such as breathing rate and heart rate, indicate the state of a person's essential body functions. They are the essential components to assess the general physical health of a person and identify various disease problems. Correlating the vital signs with our sleep quality can further enable sleep apnea diagnosis and treatment [1], treatment for asthma [2], and sleep stage detection [3]. However, the traditional way to monitor vital signs during sleep requires a patient to perform hospital visits and wear dedicated sensors [4], which are intrusive and costly. The obtained results may be biased because of the unfamiliar sleeping environments in the hospital. Moreover, it is difficult, if not possible, to run long-term sleep monitoring in clinical settings. Thus, a solution that can provide noninvasive, low-cost, and long-term vital signs monitoring without requiring hospital visits is highly desirable.

Recently, radio frequency (RF)-based monitoring solutions [5]–[8] have drawn considerable attention as they provide noninvasive breathing rate monitoring. For example, Adib *et al.* [7], [8] utilized universal software radio peripheral (USRP) and frequency modulated continuous wave (FMCW) radar to monitor a person's breathing rate by detecting the chest fluctuations caused by breathing. Doppler radar [5] and ultraband radar [6] are utilized to catch a person's breathing, respectively. These systems involve specialized devices with high complexity, which prevent them from large-scale and long-term deployment. Furthermore, Patwari *et al.* [9] and Kaltiokallio *et al.* [10] used coarse-grained channel information [i.e., received signal strength (RSS)] extracted from wireless sensor nodes to detect breathing rate. Their approach requires additional wireless network infrastructure (i.e., dedicated sensor nodes), and the coarse-grained channel information is not able to capture the vital signs of heart rate. Another new direction is using wearable sensors (such as Fitbit [11] and Jawbone [12]) to track people's fitness at any time. But they only have the capability of performing coarse-grained sleep monitoring without capturing the breathing rate, which is critical to many sleep problem diagnosis including sleep apnea. Additionally, users are required to wear these fitness sensors even during their sleep, which could be a challenge for elder people.

To address these issues, this paper aims to perform continuous long-term vital signs monitoring with low cost and without the requirement of wearing any sensor. We show that it is possible to track breathing rate and heart rate during sleep by using off-the-shelf WiFi. This will largely increase the opportunity for wide deployment and in-home use. Indeed, our system reuses existing WiFi network for tracking vital signs without dedicated/wearable sensors or additional wireless infrastructure. Furthermore, by exploiting fine-grained channel information, channel state information (CSI), provided by off-the-shelf WiFi device, our system captures not only the

Manuscript received October 16, 2017; revised February 15, 2018; accepted March 22, 2018. Date of publication April 4, 2018; date of current version June 8, 2018. This work was supported by the National Science Foundation under Grant CNS-1217387, Grant SES-1450091, Grant SES-1449958, Grant CNS-1514224, and Grant CNS-1514436. Preliminary results of this paper were presented in part at ACM MobiHoc 2015 [40]. *(Corresponding author: Yingying Chen.)*

J. Liu and Y. Chen are with the Department of Electrical and Computer Engineering, Rutgers University, Piscataway, NJ 08854 USA (e-mail: jianliu@winlab.rutgers.edu; yingche@scarletmail.rutgers.edu).

Y. Wang is with the Computer Science Department, Binghamton University, Binghamton, NY 13902 USA (e-mail: yanwang@binghamton.edu).

X. Chen is with the Department of Electrical and Computer Engineering, Rice University, Houston, TX 77005 USA (e-mail: xc20@rice.edu).

J. Cheng is with the Robert Wood Johnson Medical School, Rutgers University, North Brunswick, NJ 08902 USA (e-mail: jcheng1@rwjms.rutgers.edu).

J. Yang is with the Department of Computer Science, Florida State University, Tallahassee, FL 32306 USA (e-mail: jyang5@fsu.edu).

Digital Object Identifier 10.1109/JIOT.2018.2822818

breathing rate but also heart rate. Specifically, our system utilizes the readily available channel information to detect the minute movements caused by breathing and heart beats (i.e., inhaling, exhaling, diastole, and systole).

Using CSI has significant implication on how fine-grained minute movements can be captured for vital signs monitoring. Comparing to the traditional RSS, which only provides a single measurement of the power over the whole channel bandwidth, the fine-grained CSI provides both amplitude and phase information for multiple OFDM subcarriers. For instance, the mainstream WiFi systems such as 802.11 a/g/n are based on OFDM where the relatively wideband 20-MHz channel is partitioned into 52 subcarriers. Due to the frequency diversity of these narrowband subcarriers, the multipath effect and shadow fading at different subcarriers may result in significant difference in the observed amplitudes. This means that a small movement in physical environment may lead to the change of CSI at some subcarriers, whereas such change maybe smoothed out if we examine the signal strength over the whole channel bandwidth. Our system thus takes advantage of the fine-grained CSI provided by off-the-shelf WiFi device to capture the minute movements for vital signs monitoring.

Our system uses only a single pair of WiFi device and wireless AP for detecting the breathing rate, heart rate and sleeping patterns (e.g., sleeping events and postures) during sleep. The breathing rate detection algorithm first obtains time series of CSI from off-the-shelf WiFi device (e.g., desktop, laptop, tablet, and smartphone) and then analyzes the information in time domain and frequency domain. It achieves high accuracy for both single and two-person in bed scenarios. To detect heart rate, our algorithm first applies a bandpass filter to eliminate irrelevant frequency components, and then estimates the heart rate in the frequency domain by locating the frequency peak in the normal heart rate range. Additionally, we distinguish different sleep events (e.g., going to bed and turn overs during sleep) based on the CSI's variance energy and further identify people's sleep posture using a machine learning-based approach. Extensive experiments are conducted in laboratory environment and two apartments with difference sizes. The results show that our system provides accurate breathing rate and heart rate estimation not only under typical settings but also covering challenging scenarios including long distance between the WiFi device and AP, none-line-of-sight (NLOS) situation and different sleep postures. This demonstrates that our approach can provide device-free, continuous fine-grained vital signs monitoring without any additional cost. It has the capability to support large-scale deployment and long-term vital signs monitoring in nonclinical settings.

The main contributions of this paper are summarized as follows.

1) We show that the existing WiFi network can be reused to capture vital signs of breathing rate and heart rate through using only one AP and a single WiFi device. Such an approach can also be extended to nonsleep scenarios when the user is stationary.
2) Our proposed system extracts fine-grained CSI from off-the-shelf WiFi device to detect the minute movements and provide accurate breathing and heart rates estimation concurrently.
3) We develop algorithms that have the capability to track breathing rates of a single person as well as two-person in bed cases, which cover typical in-home scenarios.
4) The proposed system also have the capability to distinguish different sleep events and track people's sleep postures, which can help people understand their sleep status/quality.
5) Extensive experiments in both laboratory and two apartments over a three-month period show that our system can achieve comparable or even better performance as compared to existing dedicated sensor-based approaches.

The rest of this paper is organized as follows. In Section II, we put this paper in the context of the related studies. The design challenge and our system overview are described in Section III. The breathing rate estimation schemes using CSI is presented in Section IV. In Section V, we detail the proposed method of heart rate estimation. Regular sleep event and sleep posture identification is described in Section VI. We discuss the experimental setup and methodology, and present the performance evaluation results in Section VII. Finally, we conclude this paper in Section VIII.

II. Related Work

Breathing rate, heart rate, and statistics of sleep events are important indicators for evaluating one's sleep quality, stress level, and various health conditions. In general, the methods used to track such information during sleep can be categorized into four groups: 1) dedicated sensor-based; 2) smartphone and wearable sensor-based; 3) touch-free sensor-based; and 4) RF signal-based.

Traditional approaches use dedicated sensors to measure vital signs during sleep. For example, polysomnography (PSG) [4] measures body functions including breathing rate, eye movements (EOG), heart rhythm (ECG), and muscle activity by attaching multiple sensors to a patient. Such systems incur high cost and are usually limited to clinical usage. Recent advances of smartphones and wearable sensors have enabled in-home sleep monitoring by utilizing the built-in accelerometer and microphone [11]–[14]. These methods mainly provide coarse-grained monitoring including the detection of body movements, snoring, or regular sleep events, and are not able to monitor breathing rate, which is a critical indication of sleep irregularity such as sleep apnea. They also require users to place smartphones close-by and wear sensors during sleep. Recent smartphone-based approaches [15], [16] can track breathing using either earphone or acoustic FMCW on smartphones. Moreover, a more direct solution Zephyr [17] uses accelerometer and gyroscope measurements from a standard smartphone held on a person's chest for respiratory rate estimation. However, these solutions cannot provide the information of heart rate and they are also require users to place smartphones close-by even on the users' chest while asleep. Touch-free sensor-based solutions either use the sensors attached to the mattress [18] or install a camera to capture the chest movement for breathing rate estimation [19].

These systems, however, require professional installations and cannot estimate heart rate.

Most related to this paper is the RF signal-based monitoring mechanisms, such as the use of Doppler radar [5], ultrawideband [6], FMCW radar [7], [8], or RSS [9], [10], [20] for monitoring the vital signs of breathing rate. In particular, these mechanisms [5]–[8] rely on specialized hardware including USRP, FMCW radar and Doppler radar. These systems incur high cost and high complexity, making them impractical for large-scale deployment. Patwari *et al.* [9] and Kaltiokallio *et al.* [10] used RSS measurements (e.g., using 16 frequency channels in IEEE 802.15.4) extracted from wireless sensor nodes to detect the breathing rate. Their approaches require additional wireless network infrastructure and high-density placement of sensor nodes. UbiBreath [20] can track a user's breathing rate and detect apnea using RSS measurements from WiFi-enabled devices. However, the coarse-grained channel information of RSS is not able to capture the heart rate. Additionally, Nguyen *et al.* [22] used a specialized radar (i.e., iMotion radar [21]) to capture the subtle phase changes of the continuous 2.4-GHz wave signal, which are associated with a user's body movements caused by breathing, to estimate the user's breathing volume. BodyScan [23] can recognize a diverse set of human activities while also estimating the user's breathing rate, by analyzing the CSI of the radio signals transmitted/received by two designed wearable devices worn on the user's hip and wrist.

Different from the previous work, our system reuses existing WiFi network for tracking vital signs of breathing and heart rates concurrently without dedicated/wearable sensors or additional wireless infrastructure. By exploiting fine-grained CSI provided by off-the-shelf WiFi devices, our system captures both breathing rate as well as heart rate. Our system thus performs device-free, continuous fine-grained vital signs monitoring without any additional cost. It has the potential to be widely deployed in home and many other nonclinical environments.

III. System Design

In this section, we discuss the preliminaries, design challenges, and overview of our system design.

A. Preliminaries

While proliferating WiFi networks are usually used for wireless Internet access and connecting local area networks, such as an in-home WiFi network involving both mobile and stationary devices (e.g., laptop, smartphone, tablet, desktop, and smartTV), they have great potential to sense the environment changes and capture the minute movements caused by human body [24]. Indeed, WiFi signals are affected by human body movements at various scales during sleep, such as large-scale movements involving going to bed and turn over, minute movements including inhaling/exhaling for breathing, and diastole/systole for heart beats. By extracting and analyzing the unique characteristics of WiFi signals, we could capture and derive the semantic meanings of such movements including both breathing rate and heart beats during sleep. We are thus motivated to reuse existing WiFi network to monitor the fine-grained vital signs during sleep as it does not require any dedicated/wearable sensors or additional infrastructure setup.

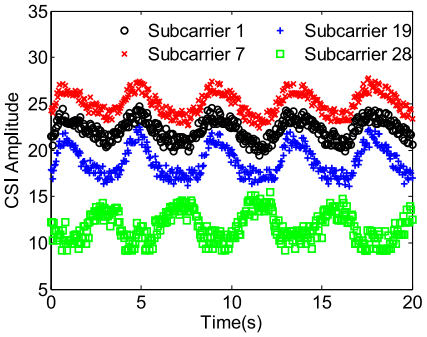

Fig. 1. CSI amplitude of four subcarriers over time when a person is asleep.

To monitor the minute movements of breathing and heart beats, we exploit the CSI provided by off-the-shelf WiFi devices as opposed to the commonly used RSS. While the coarse-grained channel information of RSS provides the averaged power in a received radio signal over the whole channel bandwidth, the fine-grained CSI of WiFi signal (based on OFDM) describes at each subcarrier how a signal propagates from the transmitter to the receiver and represents the combined effect of, for example, scattering, fading, and power decay with distance. For example, in 802.11 a/g/n, a relatively wideband 20-MHz OFDM channel (or carrier) is partitioned into 52 subcarriers. And we could examine the amplitude and phase at each subcarrier, which could be thought of as a narrowband channel, for extracting the minute movements. Due to the relative narrowband channel, the scattering and reflecting effects caused by minute movements could result in totally different amplitudes and phases at each subcarrier. Such difference, however, is usually smoothed out if we look at the averaged power over the whole channel bandwidth (i.e., RSS). Analyzing the CSI at each subcarrier thus provides great opportunity to capture the minute movements from not only breathing but also heart beats.

Fig. 1 shows the CSI amplitude of four subcarriers (i.e., subcarriers 1, 7, 19, and 28) extracted from a laptop in a 802.11n network over time when a person is asleep. His bed is in between an AP and the laptop with 3 m apart. The person does not carry any sensor in his body. We observe that the CSI amplitude of these four subcarriers exhibits an obvious periodic up-and-down trend. Such a pattern could be caused by the person's breathing during sleep. This observation strongly suggest that we may achieve device-free fine-grained vital signs monitoring by leveraging the CSI from off-the-shelf WiFi devices.

B. Challenges

Our goal is to track human vital signs of breathing and heart rates simultaneously using CSI measurements from a single pair of WiFi devices. To build such system under realistic

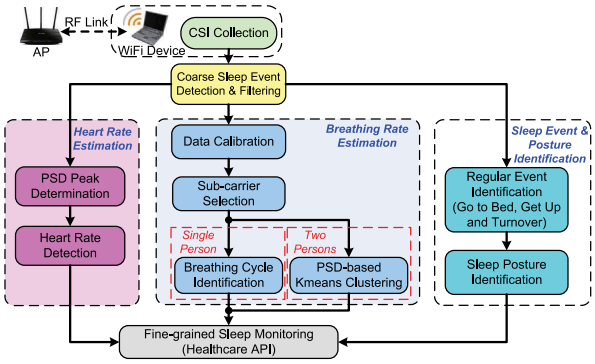

Fig. 2. Overview of system flow.

settings as a typical in-home scenario, a number of challenges need to be addressed.

1) Robustness to Real Environments: The placement of WiFi devices in real environments could change over time, and different persons present different sleeping postures. Our system should be able to provide accurate vital sign monitoring under such challenging conditions including various distances between the AP and WiFi devices, presence of walls between WiFi devices (creating NLOS scenarios), and different sleeping postures. In addition, our system should be able to identify regular sleep related events (such as turnover or getting out of bed) to facilitate vital signs monitoring.

2) Tracking Breathing and Heartbeat Simultaneously: Both breathing and heart beat only involve small body movements, presenting significant challenges when tracking such vital signs simultaneously under realistic settings. Even if the repeatable CSI changing pattern caused by breathing could be detected as shown in Fig. 1, it is difficult to capture heartbeat movements using WiFi links at the same time. Because the noisy environments will also affect CSI measurements, making it much harder to distinguish the minute movements caused by breathing (i.e., inhaling and exhaling) and heart beats (i.e., diastole and systole).

3) Sensing With Single Pair of AP and WiFi Device: Our approach should work with existing WiFi infrastructure, which may have only a single wireless link (between the AP and the device) across the human body. This presents additional challenges when two people are in-bed together. Our system should be able to distinguish and measure breathing rates coming from two people. Furthermore, the system should use WiFi traffic as little as possible, such as only utilizing existing beaconing traffic.

C. System Overview

The basic idea of our system is to track vital signs during sleep through capturing the unique patterns embedded in WiFi signals. As illustrated in Fig. 2, the system takes as input time-series CSI amplitude measurements, which can be collected at an off-the-shelf WiFi device by utilizing existing WiFi traffic or system-generated periodic traffic (if network traffic is insufficient) during people's sleep. The data is then processed to filter out the CSI measurements that contain sleep events (e.g, going to bed and turn over) or large environmental changes such as people walking by via *coarse sleep event detection and filtering*. The measurements belonging to the regular sleep events can be further classified to detailed events such as going to bed, getting off bed, and turnovers. Additionally, sleep posture plays an important role for people's sleep status/quality. For instance, some bad sleep postures (e.g., sleeping on the stomach) may be the cause of people's back and neck pain, stomach troubles [25]. The system thus would identify people's sleep posture using a machine learning-based approach via *sleep posture identification*. Moreover, this paper is based on the fact that breathing and heart rates of resting people have different frequency ranges (e.g., breathing rate ranges from 10 to 37 b/min [26], [27], and heart rate ranges from 60 to 80 b/min [28]). This useful information leads us to work on different frequency bands of the CSI measurements for accurate vital signs estimation.

The core components of our system are *breathing rate estimation* and *heart rate estimation*. After coarse sleep event detection and data filtering, based on the different frequency information embedded inside the CSI measurements, the input is fed into *breathing rate estimation* and *heart rate estimation*, respectively. In particular, the lower-frequency information of the CSI measurements is processed by the *breathing rate estimation* component. Our system first performs *data calibration* and *subcarrier selection* to preprocess the data and select only the subcarriers sensitive to minute human body movements (i.e., subcarriers with large variances). We then develop two methods, *breathing cycle* and *PSD-based K-means clustering*, to estimate the breathing rate for single and two-person in-bed scenarios, respectively. PSD denotes power spectral density (PSD). Following the similar principle, *PSD-based K-means clustering* can be easily extended to handle the case of estimating breathing rates for multiple people simultaneously given the number of people under study is known. The higher-frequency information of the CSI measurements is fed into the *heart rate estimation* component. The heart rate is then derived in the frequency domain by examining the peaks in PSD of CSI measurements. we leave the detailed presentation of *breathing rate estimation* and *heart rate estimation* to Sections IV and V, respectively.

IV. Breathing Rate Estimation

We first describe *data calibration* and *subcarrier selection*, and then present *breathing cycle identification* for estimating an individual's breathing rate. We finally show how to estimate breathing rates for two persons in-bed case.

A. Data Calibration

Data calibration is used to improve the reliability of the CSI by mitigating the noise presented in the collected CSI samples in real environments. The noise sources could come from environment-related changes, radio signal interference, etc. Our data calibration first utilizes the Hampel filter [29] to filter out the outliers which have significant different values from other neighboring CSI measurements. Specifically, we apply the Hampel filter with a sliding window at each subcarrier to remove such outliers.

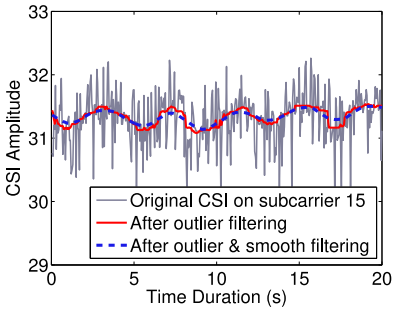

Fig. 3. Illustration of data calibration of a single subcarrier.

For CSI amplitude sequence $(x_1, x_2, \ldots, x_N)$ at each subcarrier, the Hampel identifier defines outliers as those data points x_i whose absolute difference from the median value is greater than a predetermined threshold, as defined by

$$\begin{cases} |x_i - x^*| > t \cdot M & \text{outlier} \\ |x_i - x^*| \leq t \cdot M & \text{normal measurement} \end{cases} \quad (1)$$

where i is from 1 to N, and x^* represents the median value of the rank-ordered samples of a data sequence of length N. t is a scalar threshold and M is the median absolute difference scale estimate, as defined by the following equation:

$$M = 1.4286 \cdot \text{median}\{|x_i - x^*|\} \quad (2)$$

where the constant value 1.4286 ensures that the expected value of M equals the standard deviation of normally distributed data [30].

After that, we further apply a moving average filter, which further removes high-frequency noise that is unlikely to be caused by breathing or heart beats as the corresponding minute movements usually present in a fixed frequency range. Fig. 3 illustrates the effectiveness of our data calibration by comparing the CSI amplitude before and after data calibration under an NLOS case with severe signal outliers: the CSI amplitude shown in the figure is from a single subcarrier collected from a WiFi device, which trasmits/receives packets from an AP with a wall between them. As we can see from the figure, after data calibration, the sinusoidal waves in CSI amplitude can clearly reflect the periodic up-and-down chest and belly movements caused by breathing.

B. Subcarrier Selection Strategy

We observe that the amplitudes of different subcarriers have different sensitivity to inhaling and exhaling caused by breathing due to frequency diversity. Fig. 4(a) presents an example of CSI amplitude over time on 30 subcarriers extracted from a laptop in WiFi network when a person is asleep. We find that the CSI from the smaller subcarrier indices is significantly affected by the minute movements caused by breathing, while CSI from the higher subcarrier indices (i.e., from 15 to 30) is less sensitive. This is because different subcarriers have different central frequencies, which have different wavelengthes. Combining the effect of multipath/shadowing with different frequencies, CSI measurements at different subcarriers thus have different amplitudes. Those subcarriers not sensitive to the breathing activity should be filtered out. We utilize the

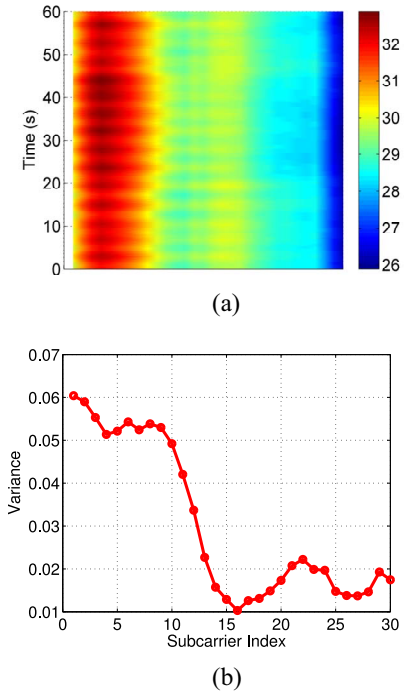

Fig. 4. Example of CSI amplitude pattern at 30 subcarriers and the corresponding variance. (a) CSI time series patterns after data calibration. (b) Variance of each subcarrier.

variance of CSI amplitude in a moving time window to quantify the subcarrier's sensitivity to minute movements. Fig. 4(b) shows the variance of 30 subcarriers. We can see that subcarriers with higher variance are more sensitive to minute movements. We thus use a threshold-based method to select subcarriers having large variance of CSI amplitude in a time window for breathing rate estimation.

C. Breathing Cycle Identification

As breathing involves periodic minute movements of inhaling and exhaling, our breathing cycle identification aims to capture the periodic changes in CSI measurements caused by breathing. From Fig. 1, we observe the CSI amplitude on the selected subcarrier indeed presents a sinusoidal-like periodic changing pattern over the time due to breathing. This observation suggests that we can identify breathing cycles by measuring the peak-to-peak time interval of sinusoidal CSI amplitudes. We thus first identify peaks of sinusoidal CSI amplitude patterns to calculate peak-to-peak intervals. We then combine the peak-to-peak intervals from multiple subcarriers to improve the robustness and the accuracy of breathing cycle identification.

1) Local Peak Identification: A typical peak finding algorithm determines a data sample as a peak if its value is larger than its two neighboring samples. However, such simple method produces many *fake peaks* (i.e., the identified peaks that are not at the location of real peaks of the sinusoidal CSI amplitude pattern) as illustrated in Fig. 5. The peak τ_5 has larger value than its two neighboring samples, yet, it is a fake peak among these nine identified peaks. In order to filter out

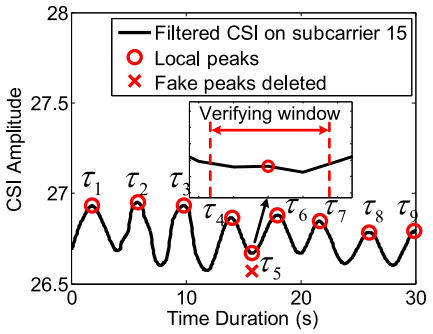

Fig. 5. Illustration of fake peak removal.

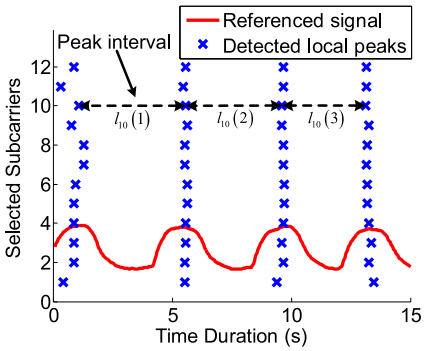

Fig. 6. Local peaks of all selected subcarriers.

Algorithm 1 Fake Peak Removal

Require:
CSI time series on subcarrier i: $c_i = \{c_i(1), ..., c_i(M)\}$;
Local peak set: $MaxSet = \{\tau_k, 1 \leqslant k \leqslant K\}$;
Length of the verifying window: N;
Ensure:
$MaxSet$ after removing fake maximums;
1: **for** k=1: K **do**
2: $locs$:= location(τ_k);
3: amp := amplitude(τ_k);
4: **for** $m := locs\text{-}\left\lfloor \frac{N-1}{2} \right\rfloor : locs\text{+}\left\lfloor \frac{N-1}{2} \right\rfloor$ **do**
5: **if** $m < 0 \parallel m > M$ **then**
6: **continue**;
7: **end if**
8: **if** $amp < c_i(m)$ **then**
9: delete τ_k from $MaxSet$;
10: **break**;
11: **end if**
12: **end for**
13: **end for**
14: **return** $MaxSet$;

the fake peaks, we apply a threshold to the minimum distance between two neighboring peaks based on human's maximum possible breathing rate. In addition, we develop a *Fake Peak Removal* algorithm to further reduce the number of fake peaks.

Specifically, adults usually breathe at 10–14 breathes per minute (b/min) [27], while new born babies breathe at around 37 b/min [26]. We therefore set the range of breathing rates being considered in this paper to 10–37 b/min, which covers a broad range including fast and slow breathing rates. We further adopt a minimum acceptable interval σ_{mpd} that corresponds to the maximum possible breathing rate as a threshold to remove the peaks that are too close to each other. If a peak has its backward interval (i.e., the interval between previous peak and current peak) less than the minimum acceptable interval length, it will be identified as a fake peak. In particular, we set the minimum acceptable interval $\sigma_{\text{mpd}} = 60 \cdot f/37$ samples, which corresponds to the maximum possible breathing rate for infants. The parameter f is the sampling rate of CSI measurements that corresponds to WiFi packet transmission rate.

In addition, we confirm the identified peaks by comparing its value to multiple data samples within a verification window centered at the peak. The system only keeps the identified peak when its value is greater than all the data samples in the verification window. The algorithm of fake peak removal is provided in Algorithm 1. In our experiments, we observe that a short verification window of 1 s is good enough to remove fake peaks.

2) Breathing Cycles Combination: Once we capture all the local peaks from the selected subcarriers, a more clear pattern can be obtained as shown in Fig. 6. The referenced signal is derived from the NEULOG Respiration Monitor Logger Sensor [31], which is connected to a monitor belt attached to the user's ribcage while asleep. Next, our system estimates the breathing rate by combining peak-to-peak intervals obtained crossing all selected subcarriers. We denote a set of peak-to-peak intervals obtained from P selected subcarriers as $L = [l_1, \ldots, l_i, \ldots, l_P]'$, where $l_i = \{l_i(1), \ldots, l_i(N_i - 1)\}$ is a vector of N_i peak-to-peak intervals obtained from the ith subcarrier. Then the estimated breathing cycle E_i from the ith subcarrier can be obtained by using the following equation:

$$\arg\min_{E_i} \sum_{n=1}^{N_i-1} |E_i - l_i(n)|^2. \tag{3}$$

Considering the subcarriers with larger variance are more sensitive to the minute movements, we utilize a weighted mean of estimated breathing cycles crossing all selected subcarriers to obtain a more accurate estimation of breathing cycle E, which is defined as follows:

$$E = \sum_{i=1}^{P} \frac{\text{var}(c_i) \cdot E_i}{\sum_{i=1}^{P} \text{var}(c_i)} \tag{4}$$

where P is the number of validated subcarriers and c_i is the CSI amplitude measurements on the ith subcarrier. The breathing rate finally can be identified as $60/E$ b/min.

D. Breathing Rate Estimation of Two Persons Scenario

Estimating breathing rate becomes challenging when there are two persons in bed as the CSI measurements would be affected by two independent movements simultaneously due to breathing. It is hard to observe a clear sinusoidal pattern in the time series of CSI amplitude. Nevertheless, the frequency of the breathing coming from two persons is still preserved if we transfer the time series of CSI to the frequency domain. We therefore develop a mechanism to determine two people's breathing rates simultaneously by examining the frequency components in CSI measurements.

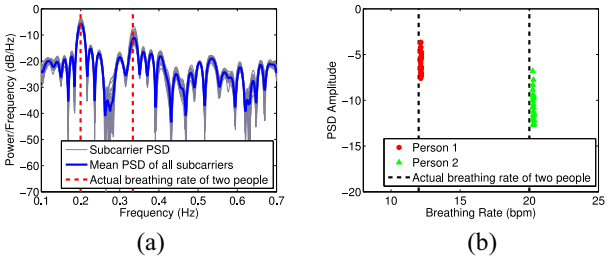

Fig. 7. Illustration of two people breathing at different frequencies (12 b/min and 20 b/min). (a) PSD of CSI measurements. (b) *K*-means clustering of subcarriers' peaks.

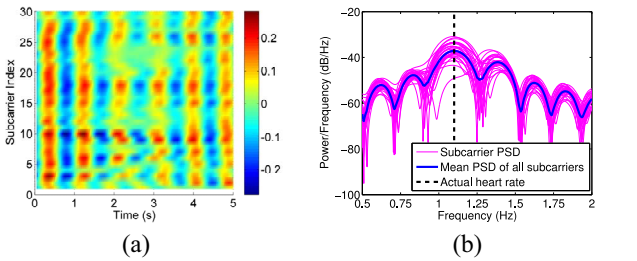

Fig. 8. Recovered heart beats by applying pass band filtering and PSD of CSI measurements. (a) CSI time series patterns. (b) PSD of CSI measurements on all subcarriers.

In particular, our system analyzes the time series of CSI amplitude in frequency domain by using the PSD. The PSD transforms the time series of CSI measurements on each subcarrier to its power distribution in the frequency domain. It is used to identify the frequencies having strong signal power. A strong sinusoidal signal generates a peak at the frequency corresponding to the period of the sinusoidal signal in PSD. Therefore, the CSI amplitude measurements collected when two persons in bed should present two strong peaks at the frequency corresponding to the breathing rate of two persons, respectively. The PSD on the *i*th subcarrier with *N* CSI amplitude measurements can be calculated with the following equation:

$$\mathrm{PSD}_i = 10\log_{10}\frac{(abs(\mathrm{FFT}(\mathrm{c_i})))^2}{N} \tag{5}$$

where c_i is the vector of CSI measurements on subcarrier i.

For each selected subcarrier, we utilize a threshold-based approach to identifying the candidate peaks within its PSD. We then use a *K*-means clustering method to classify the candidate peaks into two clusters based on 2-D feature including PSD amplitude and corresponding frequency. The number of targeted people (i.e., K in K-means) can be either estimated using existing work (e.g., [32]) or entered manually from the users. The average values of the frequencies in two clusters are identified as the breathing rates of these two people. Fig. 7 shows an example of estimating two persons' breathing rate using PSD-based method. The ground truths of two persons' breathing rates are 12 and 20 b/min (i.e., 0.2 and 0.33 Hz, respectively). Fig. 7(a) depicts that there are two strong peaks in the PSD of selected subcarriers near these two frequencies, respectively. Fig. 7(b) shows that our PSD-based *K*-means clustering method can effectively estimate the breathing rates of two persons in bed simultaneously. We note that the proposed approach still works even when two people have the same breathing rates. Under such scenario, our approach returns two close-by PSD peaks on each selected subcarrier in the frequency domain after *K*-means clustering. In addition, the person's chest or belly that is closer to the wireless link has bigger impact on the CSI changes, which creates more obvious periodic changes of CSI. This leads to the stronger peak corresponds to that person's breathing or heart beat rate. We thus can map the detected breathing or heart rates to each individual based on the strength of the peak and the proximity of the individual to the wireless link.

V. Heart Rate Estimation

Heart rate is a very important indicator of the persons' sleep status, quality and overall health condition. While the breathing patterns can be observed in the CSI measurement, the heart rates do not produce observable periodic CSI change patterns in the time series CSI measurements. This is because the vibration of blood vessels caused by heart beat (i.e., diastole and systole) are smaller minute movements than that of breathing. Thus, the effect of minute movement of heartbeat is overlapped with and covered by the chest and belly movements of breathing. On the other hand, the heartbeat has much higher frequency than breathing. We thus can filter out the interference of breathing in order to facilitate the heart rate estimation.

In particular, after coarse sleep event detection and filtering, the CSI measurements with the frequency range related to normal heart rate range of resting people (i.e., 60–80 b/min, which corresponds to 1–1.33 Hz) will be separated and served as input to our Heart Rate Estimation. The patterns of CSI measurements of all subcarriers after such band-pass filtering are illustrated in Fig. 8(a), from which we can observe the CSI changing that accompany the heart beats. With the aid of the band-pass filter, the mean PSD curve for all subcarriers displays a noticeable peak in the PSD graph at the frequency of 1.095 Hz, namely 65.7 b/min, in Fig. 8(b). In the same figure, there is a black dashed line representing the ground truth of 66 b/min measured by a commercial fingertip pulse sensor during such time period. We then analyze the CSI amplitude on each subcarrier in frequency domain and generate the PSD [refer to (5)] to identify the frequencies having strong signal power. We can thus determine the heart rate by locating the maximum power in the average PSD of all subcarriers in the normal heart rate range. For two person's heart rates monitoring, we can identify two heart rates simultaneously by using the similar approach to the breathing rate estimation of two persons illustrated in Section IV-D.

In addition to heart rates, fine-grained heart movement metrics (e.g., the heart rate variability and R-R interval) have been shown to be good predictors for many possible heart diseases [33]. We find that the normalized CSI can well capture the detailed heart movement information from WiFi signals. Particularly, we preprocess the raw CSI readings on each subcarrier via the aforementioned band-pass filter, and sum each subcarrier's readings together to get the normalized CSI. In the

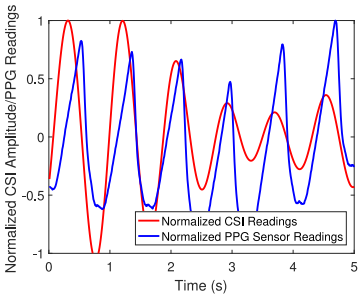

Fig. 9. Comparison of normalized CSI patterns and PPG sensor readings.

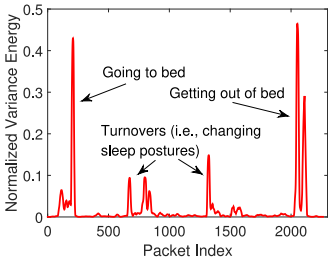

Fig. 10. Short time energy of the variance of difference sleep events.

experiment, we placed the WiFi device and AP at two sides of the bed with the distance of 5 ft, and the line-of-sight between the WiFi device/AP is crossing the person's chest, so that our system can well capture the user's minute body movements associated with the heart beats. Due to the vibrations of blood vessels caused by the diastole and systole of a heart, the human body usually has slight movements when the heart beats. Similar to the body movements caused by breathing, the even smaller movements associated with heart beats also result in different amplitudes and phases at each subcarrier of WiFi signals. After the band-pass filtering with the pass band limited to the frequency range of human heart rate, the peaks/valleys in the CSI patterns can be used to measure the heart contracts and cardiac diastole motions. Fig. 9 compares the normalized CSI patterns to a wrist-worn photoplethysmogram (PPG) sensor's readings when the user is asleep. The PPG sensor is usually used in clinical scenarios for collecting accurate heart rates and detailed heart movement metrics. From Fig. 9, we can see that the changing pattern of the normalized CSI is highly correlated with the readings from the PPG sensor, indicating that the normalized CSI obtained from WiFi signals could be utilized to extract the fine-grained heart movement metrics such as heart contracts and cardiac diastole (i.e., peak/valley in the corresponding CSI patterns [34]).

VI. Sleep Event and Sleep Posture Identification

A. Coarse Sleep Event Detection and Environmental Change Filtering

Coarse sleep event detection and filtering is used to detect and filter out the sleep events or environmental changes that interfere with the minute movements of breathing and heart beat during sleep. These sleep events, such as turnovers (i.e., changing sleeping postures) and getting up, and occasional changes of environments, such as people walking by, involve large-scale body movements which significantly affect the CSI measurements and are irrelevant to vital signs monitoring. Our system thus performs coarse determination of CSI segments containing such inference factors and filters them out to facilitate accurate vital signs monitoring during sleep.

In particular, we employ a threshold-based approach to determine whether a segment of CSI measurements contains sleep events/environmental changes or not by examining the short-time energy of the moving variance of the CSI measurements. The rationale behind this is that the sleep events or environmental changes involving large body movements (e.g., going to bed and turn over) result in much larger changes of CSI measurement than that of minute movements of breathing and heart beat. The large movements thus can be detected once the variance energy of the corresponding CSI measurements exceeds a particular threshold.

We denote the CSI samples of P subcarriers as $C = [C_1, \ldots, C_p, \ldots, C_P]'$, where $C_p = \{c_p(1), \ldots, c_p(T)\}$ represents T CSI amplitudes on the pth subcarrier. We further denote the moving variances of the P subcarriers as $V = [V_1, \ldots, V_p, \ldots, V_P]'$, where $V_p = \{v_p(1), \ldots, v_p(T)\}$ are the moving variances derived from C_p. Our system can then calculate the cumulative moving variance energy of CSI samples accessing P subcarriers as

$$E = \frac{1}{NP} \sum_{p=1}^{P} \sum_{n=1}^{N} \left| v_p(n) \right|^2 \tag{6}$$

where N denotes the window length of short time energy.

We empirically determine the variance energy to be 0.02 as the threshold in this paper. Fig. 10 illustrates the normalized moving variance energy of CSI measurements that are collected when the participant involves different sleep events during sleep. We observe that all sleep events generate significantly large variance energy comparing to that of the minute movements of only breathing and heart beats.

B. Regular Sleep Event Identification

Given the detected sleep events, we further classify them into detailed events such as going to bed, getting off bed, and turnovers. Generating statistic of such detailed events can help quantify the sleep quality. For example, frequent getting up or turning overs may suggest that the person has difficulty falling asleep. This information contributes to many healthcare applications such as elderly care and medical diagnosis. As shown in Fig. 10, sleep events involving relative larger-scale movements (i.e., going to bed and getting out of bed) result in much larger variance energy than those involving relative smaller-scale movements (i.e., turn overs). We thus can distinguish sleep events with larger-scale movements from those with smaller-scale movements by comparing the variance energy from (6). To further distinguish larger-scale movements, we can exploit the changes of the number of persons in bed to infer these two events. The number of persons in bed can be obtained by using a profile-based approach as studied in existing work (e.g., [32]).

C. Sleep Posture Identification

Sleep posture/position also plays an important role on a good night's sleep. A comfortable sleep posture could make a

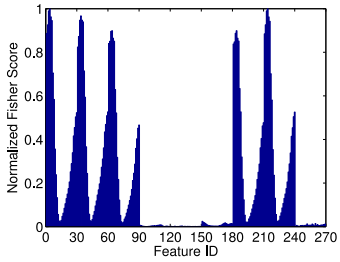

Fig. 11. Derived Fisher score of the extracted 270 features on 30 subcarrier groups (features 1–30 are the first feature *mean* on 30 subcarrier groups, and so on so forth).

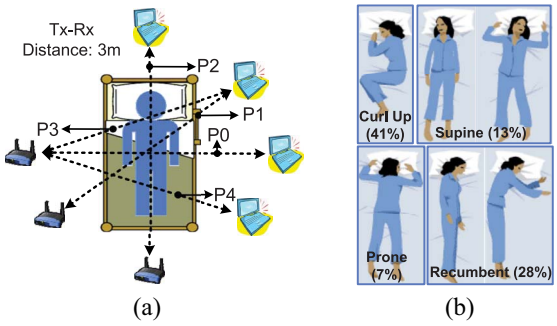

Fig. 12. Setup of relative position of WiFi device and AP and sleeping postures. (a) Setup of WiFi device-AP pair with different relative positions. (b) Different sleep postures in bed [35].

person easier to align his head, neck, spine, and keep them in a neutral position, whereas some bad sleep postures (e.g., sleeping on the stomach) may be the cause of people's back and neck pain, stomach troubles, etc. [25]. Moreover, some researchers also found that different sleep postures incur different health effects. For example, the freefall posture is good for digestion, while the starfish and soldier positions are more likely to lead to snoring and a bad night's sleep [35]. This encourages us to identify and track people's sleep postures using WiFi signals, which could provide additional sleep information to assist identifying potential reasons of sleep difficulty or health problems. Intuitively, different sleep postures have inevitable influence to WiFi signals, therefore we propose to match the features extracted from CSI with the trained profiles to differentiate sleep postures.

1) Feature Extraction and Selection: In particular, we use a sliding window whose length is 5 s on the calibrated CSI time series (after the *data calibration* that is discussed in Section IV-A) and extract nine basic features including *mean, maximum, minimum, variance, skewness, range, mode, median*, and *kurtosis* on each subcarrier group. Therefore, for the 30 subcarrier groups, we could have 270 features in total for each time window. In addition, since not all wireless signal transmission paths would be influenced by people's different postures, we find that only a few subcarriers or features are distinguishable enough to differentiate these sleep postures. We thus select a subset of features that are more unique between different sleep postures from the 270 extracted features on 30 subcarrier groups based on Fisher score [36]. The Fisher score of the ith feature is defined as follows:

$$F_i = \frac{\sum_{j=1}^{c} n_j \left(\mu_j - \mu\right)^2}{\sum_{j=1}^{c} n_j \delta_j^2} \tag{7}$$

where n_j is the number of instances in sleep posture class j, $j = 1, \ldots, c$, μ_j and δ_j^2 denote the mean and variance of class j corresponding to the ith feature, and μ denotes the mean of ith feature candidates in the whole training data sets. Fig. 11 shows the normalized Fisher scores of those 270 features spanning on 30 subcarrier groups that we extract to discriminate different sleep postures. Fig. 11 shows the normalized Fisher scores of the nine types of features extracted from 30 subcarrier groups, every 30 Fisher scores in this figure correspond to one type of the features. From the figure, we observe that, for a particular type of feature, not all the subcarriers have high Fisher scores (e.g., presenting a V-shape pattern), which means they are not equally sensitive to human body movements. Note that such sensitivity differences are often caused by the relative position of the AP and WiFi device to the human body. In addition, we observe that the features *variance, skewness, range*, and *kurtosis* (i.e., feature IDs 91–180 and 241–270) with low Fisher score are not representative for each posture. In order to reduce the impact of nonsensitive features and subcarrier groups to the sleep posture identification, we empirically choose a threshold (i.e., $\tau_f = 0.1$) and only use the features having Fisher scores larger than the threshold for the sleep posture identification.

2) PCA Dimension Reduction: In order to further reduce the computational cost in the later classification process, we adopt principal component analysis (PCA) [37] which not only converts original feature vectors into a set of linearly uncorrelated principal components but also removes uncorrelated noise components in the features. Specifically, we adopt PCA to convert the selected features in each time window into 20 linearly uncorrelated principal components.

3) Posture Training and Identification: Our system mainly focus on identifying four typical sleep postures, including *curl up, supine, prone,* and *recumbent*, which are illustrated in Fig. 12(b). Given a specific WiFi device setup, our system first constructs the four sleep posture profiles with the extracted CSI features. Then the four posture profiles are, respectively, used to train a machine learning-based classifier. Finally, in the sleep posture identification phase, CSI measurements and their corresponding features collected while the user is sleeping are fed into the classifier to identify the user's posture. We compared the performance of using four different classifiers including discriminant analysis (DA), k-nearest neighbors (k-NN), support vector machine (SVM), and random forest (RF), which are described in Section VII.

VII. Performance Evaluation

In this section, we evaluate our system of tracking vital signs during sleep in both laboratory and two apartments.

A. Device and Network

We conduct experiments in an 802.11n WiFi network with a single off-the-shelf WiFi device (i.e., Lenovo T500 Laptop) connected to a commercial wireless access point (AP) (i.e., TP-Link TL-WDR4300). The laptop runs Ubuntu 10.04 LTS

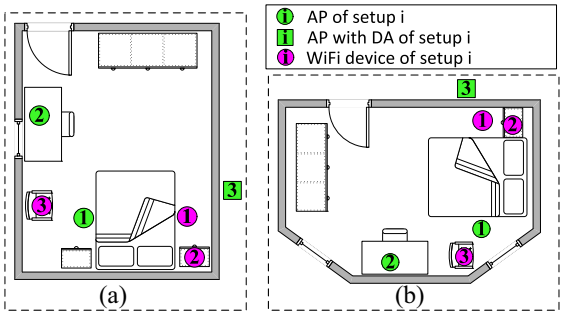

Fig. 13. Two apartment setup.

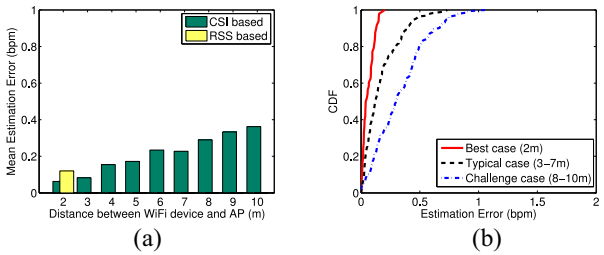

Fig. 14. Performance under different distances between WiFi device and AP. (a) Mean estimation error. (b) CDF of estimation error.

with the 2.6.36 kernel and is equipped with an Intel WiFi Link 5300 card for measuring CSI [38]. Unless mentioned otherwise, the packet transmission rate is set to 20 pkts/s. How the packet rate affects the performance will be discussed in Section VII-F4. For each packet, we extract CSI for 30 subcarrier groups, which are evenly distributed in the 56 subcarriers of a 20-MHz channel [38].

B. Experimental Methodology

The experiments are conducted in both laboratory and two apartments with six participants over a three-month time period. The laboratory environment is a large room with office cubic around. It is used to study the impact of various factors such as obstacles, the various distances between the AP and the WiFi device, and sleep postures. In breathing rate estimation experiments, the participants lie on a bed and control their breathing rate to follow various steady beats from a metronome, which is set to a rhythm ranging from 12 to 18 b/min.

We also conduct experiments in two apartments with different bedroom sizes. Fig. 13 illustrates the environmental setup in two bedrooms, in which both beds are queen size. The smaller one (i.e., bedroom 1) has the size of about 12 ft $\times$ 9 ft, whereas the larger one (i.e., bedroom 2) is about 15 ft $\times$ 12 ft. As shown in Fig. 13, we have three setups in both apartments: setup 1 is the ideal scenario where the AP and WiFi device are placed at two sides of the bed. This setup is useful for persons who want to optimize the performance of the vital signs monitoring during sleep. Setup 2 represents a typical scenario where there is an AP inside the room and a WiFi device, such as smartphone, laptop, or tablet, is put on the bed table. Setup 2 has larger distance between the AP and the WiFi device than setup 1. Setup 3 is a challenging scenario where the AP and the WiFi device are placed in different rooms with a concrete wall between them. The distance between the AP and the WiFi device is the largest among three setups. In this setup, we utilize directional antennas (i.e., TL-ANT2406A) to enhance the reception of WiFi signals. Specifically, the distances between the AP and the WiFi device in the three setups of the bedroom 1 are 5, 13, and 11 ft, respectively. And the distances in the three setups of the bedroom 2 are 5, 14, and 12 ft, respectively. The ground truths of breathing and heart rates are monitored by the NEULOG Respiration Monitor Logger Sensor [31] and a fingertip pulse oximeter, respectively.

For the sleep posture identification experiments, we collect the CSI measurements when a participant lies in bed in the laboratory environment and perform four common sleep postures, which include prone, supine, curl-up, and recumbent as shown in Fig. 12(b). The participant stayed in each posture for about 40 min. The relative position of the AP/WiFi device to the human body is same as the setup 2 in Fig. 13(a), and the distance of the AP and WiFi device is around 10 ft.

C. Evaluation of Breathing Rate Estimation

We evaluate the overall performance of breathing rate estimation under different scenarios including different distances between the AP and the WiFi, evaluation in two real apartments and two persons in bed case.

1) Effect of Device Distance: As typical bedroom has limited space, we choose a large laboratory environment to study the performance of breathing rate estimation under various distances. The AP and the WiFi devices are placed at two sides of the bed [i.e., *P*0 setup in Fig. 12(a)] with distances from 2 to 10 m. Fig. 14(a) presents the mean error in terms of b/min of breathing rate estimation under different distances when there is a single person in bed. Overall, we observe that the mean estimation error of our breathing rate estimation is lower than 0.4 b/min, which demonstrates that our system is very accurate across different distances including very large distances such as 5–10 m. In addition, shorter distance between the AP and the WiFi device results in better performance. For example, the mean error is within 0.2 b/min when the distance is under 5 m. This is because the received WiFi signals are stronger with shorter communication distances, providing more reliable measurements to capture the minute movements of breathing. Comparing to the result of existing work using RSS [10] which only tested with the distance of 2 m, as shown in yellow bar in Fig. 14(a), our system provides significantly better performance (i.e., the error is reduced by about 67%).

Fig. 14(b) depicts the cumulative density function (CDF) of the breathing rate estimation error for three categories of distances between the AP and WiFi device: 1) *best case* (i.e., 2 m); 2) *typical case* (i.e., 3–7 m covering mid-sized bedrooms); and 3) *challenging case* (i.e., 8–10 m covering huge-sized bedrooms). As we can see that for both *best case* and *typical case*, over 90% estimation errors are less than 0.4 b/min. Even for the *challenging case*, over 80% of estimation errors are smaller than 0.5 b/min. This suggests that

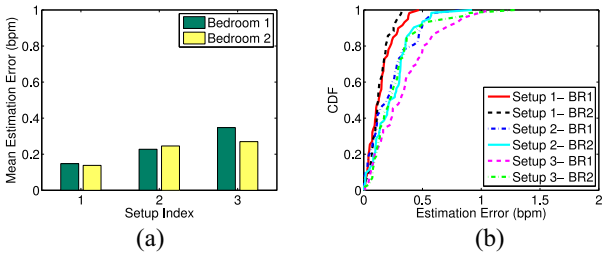

Fig. 15. Performance in two real apartments. (a) Mean estimation error. (b) CDF of estimation error.

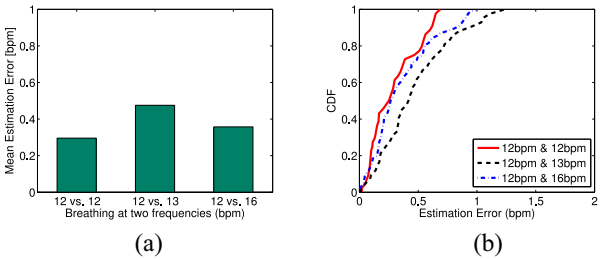

Fig. 16. Breathing rate estimation of two persons in bed. (a) Mean estimation error. (b) CDF of estimation error.

our system can achieve highly accurate breathing rate estimation by using a single pair of AP and WiFi device. And it supports large distance between them.

2) Evaluation in Real Apartments: We next evaluate the breathing rate estimation in two different-size apartment bedrooms with different deployments of the AP and WiFi device, as shown in Fig. 13. Fig. 15(a) presents the mean estimation error for each setup in two bedrooms. We find that the setup 1 achieves the lowest estimation error of about 0.15 b/min in both bedrooms due to the shortest distance between the AP and WiFi devices. The estimation error of setup 2 increases as the distance between two devices increases. Still, setup 2 has the estimation error as low as 0.22 and 0.24 b/min in bedrooms 1 and 2, respectively. In addition, we observe that although setup 3 involves the obstacle (i.e., a 6-in wall) that blocks the line-of-sight signal transmission and longer distance between the AP and WiFi devices, we can still achieve less than 0.3-b/min mean estimation error with a single pair of AP and WiFi device. Moreover, Fig. 15(b) shows that more than 80% estimation errors are less than 0.5 b/min for all of those three setups in two real bedrooms, indicating that our system is accurate and robust in real apartment environments. The above results show that our system provides effective breathing rate monitoring under various distances of WiFi device and AP and is robust across different environments.

3) Two Persons in Bed Case: We further test our system with two persons in bed using bedroom 1 setup. The AP and WiFi device are placed at two sides of the bed with the distance of 3 m. Two participants are breathing with different rates as: {12, 12 b/min}, {12, 13 b/min}, and {12, 16 b/min}. Fig. 16 depicts the mean estimation error and the CDF of the breathing estimation error. We observe that the mean error is within 0.5 b/min for all combination of different breathing rates. In addition, we find that over 90% of estimation errors

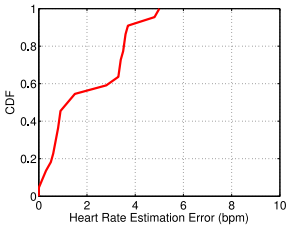

Fig. 17. Performance of heart rate estimation.

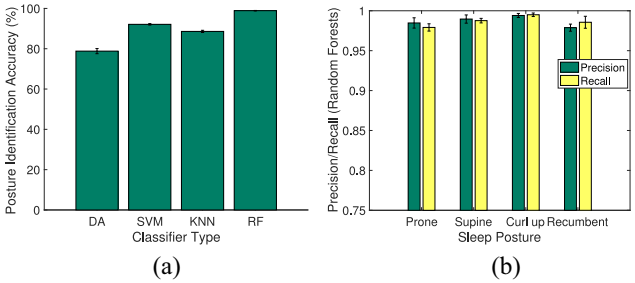

Fig. 18. Performance of sleep posture identification. (a) Posture classification accuracy. (b) Precision/recall of posture identification.

are less than 1 b/min, which is comparable to that of commercial physical contact devices (e.g., zephyr [39]). Given that we only use a single pair of AP and WiFi device, such accuracy of breathing rate monitoring is very encouraging.

D. Performance of Heart Rate Estimation

Fig. 17 illustrates the CDF of heart rate estimation error when one person is in bed using setup 1 in bedroom 1 with the AP equipped with directional antennas. We observe that about 57% of estimation errors are less than 2 b/min and over 90% of estimation errors are less than 4 b/min. The results are very encouraging as our system achieves comparable accuracy to that of commercial sensors, e.g., Zephyr [39] and SleepIQ [18]. Comparing with these commercial products, our system reuses existing WiFi network without dedicated/wearable sensors or additional cost. Our system thus is able to support large-scale deployment and long-term vital signs monitoring in nonclinical settings. To the best of our knowledge, this paper is the first to achieve device-free heart rate estimation leveraging off-the-shelf WiFi.

E. Performance of Sleep Posture Identification

We adopt a variety of machine learning classifiers to perform sleep posture identification, including DA, SVMs with linear kernel, k-NNs ($K = 5$), and RFs. Fig. 18(a) presents the overall accuracies of sleep posture recognition models built upon multiple classifiers. We find that all classifiers yield the accuracies over 80%. Specifically, k-NN ($K = 5$), SVM, and RF classifiers result in the sleep posture identification accuracies over 90%, which also verifies the robustness of aforementioned feature extraction and selection techniques. We then look into the precision and recall rates of our sleep posture recognition model trained by the RF that outperforms all other classifiers, which are shown in Fig. 18(b). We notice that even the lowest precision and recall rates across all four sleep postures are still higher than 0.95, which again

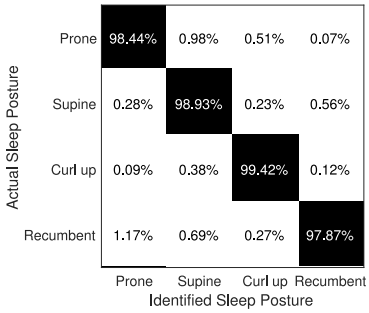

Fig. 19. Confusion matrix of sleep posture identification.

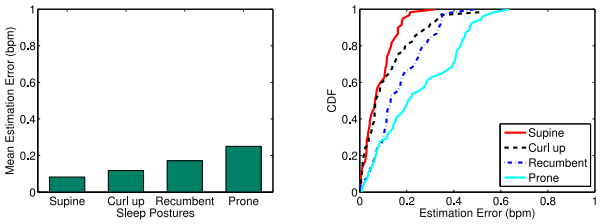

Fig. 20. Impact of sleep postures on the breathing rate estimation. (a) Mean estimation error. (b) CDF of estimation error.

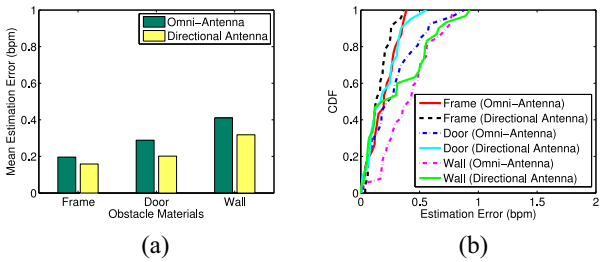

Fig. 21. Impact of the types of obstacles between WiFi device and AP on the breathing rate estimation. (a) Mean estimation error. (b) CDF of estimation error.

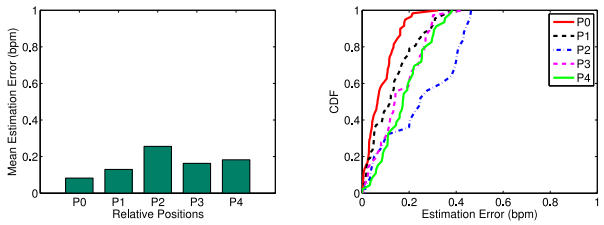

Fig. 22. Effect of relative position of WiFi device and AP. (a) Mean estimation error. (b) CDF of estimation error.

demonstrates the decent accuracy achieved by our system in identifying user various sleep postures in bed.

We further examine the confusion matrix that describes the identification accuracy for each of four sleep postures using the RF classifier, which is shown as Fig. 19. Each row represents the actual user sleep posture and each column shows the posture that is predicted by our system. Each cell in this confusion matrix contains the percentage of the actual user sleep posture in the row that is classified as the postures in the column. We note that our sleep posture classification model using RFs can estimate each of sleep postures with accuracy over 98%. The above evaluation results collectively show that our system is able to estimate user sleep postures with high accuracy using a single pair of WiFi devices.

F. Impact of Various Factors

In this section, we perform detailed study of breathing rate estimation under various factors.

1) Sleep Postures: We experiment with different sleep postures as shown in Fig. 12(b). The AP and laptop are placed at two sides of the bed with the distance of 3 m. Fig. 20(a) compares the mean error of breathing rate estimation resulted from different sleep postures. Overall, our system achieves less than 0.3-b/min mean error for all sleep postures, which demonstrates the effectiveness and robustness of our system. In particular, the mean estimation errors of supine, curl up, and recumbent positions are about 0.07, 0.1, and 0.158 b/min, respectively. Fig. 20(b) shows the CDF curves of estimation error for all postures. We find that our system can obtain less than 0.2-b/min error for more than 80% of typical sleep postures. The prone posture has the largest mean estimation error of about 0.25 b/min for the reason that the body movements, which are caused by breathing, are mainly in the chest and belly and would be absorbed and blocked by the soft mattress. Still, our system achieves 93% of estimation errors less than 0.5 b/min for prone posture.

2) Obstacles/Walls: We evaluate our system with obstacles of different materials in between of AP and WiFi device with *P*0 deployment in Fig. 12(a). These obstacles are commonly used materials in home environments including a plastic frame of 1 in, a solid wood door of 2 in, and a concrete wall of 6 in. As more and more people use directional antenna to boost the wireless signal reception in home WiFi network, we use both directional and omnidirectional antennas in the experiments. From Fig. 21(a), we observe that the mean error is less than 0.4 b/min for all materials. Obviously, with the concrete wall, the performance is slightly worse than that of door and plastic frame. In addition, by using the directional antenna, the mean error decreases about 0.1 b/min, indicating the directional antenna can enhance the performance of breathing rate estimation due to stronger received signals. Fig. 21(b) shows the CDFs of estimation error. We observe that the error is always within 0.5 and 1 b/min for the plastic frame and wall, respectively. The results show that our system can work under different obstacles and the directional antenna could improve the performance. A more comprehensive study of the system performance in various environments with more obstacles and walls will be presented in our future work.

3) Relative Position of WiFi Device and AP: Fig. 22(a) shows the mean error of breathing rate estimation under different relative positions of Tx–Rx pair (i.e., the AP and WiFi device), as shown in Fig. 12(a). We find that the deployment *P*2 has the largest mean error at about 0.26 b/min among all deployments (i.e., *P*0–*P*4) since the WiFi signals are partially blocked by the human body (i.e., head and feet). In addition, Fig. 22(b) depicts the CDFs of breathing rate estimation errors. We observe that the estimation errors are all within

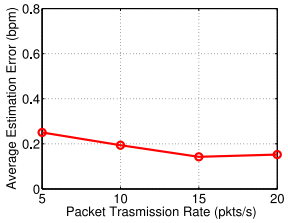

Fig. 23. Effect of packet transmission rate.

than 0.5 b/min even for the worst case deployment *P*2. Above results show that our system is effective under different relative positions of WiFi device-AP pair.

4) Packet Transmission Rate: As higher packet transmission rate results in more CSI measurements for vital signs monitoring, we are interested in how the packet rate affects the performance of our system. Furthermore, we study whether our system can work with existing WiFi beaconing packets. Fig. 23 presents the mean breathing rate estimation error versus packet transmission rate when varying the transmission rate from 5 to 20 pkt/s using the dataset from apartment experiment (i.e., bedroom 1 and setup 1). We observe that high packet transmission rate slightly improves the performance. Overall, our system is not very sensitive to packet transmission rate, given the range from 5 to 20 pkt/s. Specifically, when the packet transmission rate is as low as 5 or 10 pkts/s, our system has about 0.24- and 0.2-b/min mean estimation error, respectively. As the commercial APs have the beaconing of 10 pkts/s to broadcast their SSID, our system is able to use such beacons for accurate breathing rate estimation. These results show that our system cannot only work with existing AP beaconing packets but also provide accurate breathing rate monitoring with even less packet rate, such as 5 pkts/s.

VIII. Conclusion

In this paper, we show that the WiFi network could be exploited to track vital signs during sleep including breathing and heart rates using only one AP and a single WiFi device. In particular, our system exploits fine-grained CSI from off-the-shelf WiFi devices to detect the minute movements associated with breathing and heartbeat activities. Our algorithms grounded on CSI information in both time and frequency domain have the capability to estimate the breathing rate of a single person as well as two-person in bed cases. Additionally, the existing WiFi links can also be used to track people's sleeping events (e.g., turnovers and getting up) and sleeping postures. Extensive experiments in both laboratory and two apartments confirm that our proposed approach using the existing WiFi network can achieve comparable or even better accuracies as compared to existing dedicated sensor-based approaches. This WiFi-based approach opens up a new direction in performing device-free and low-cost vital sign monitoring during sleep in nonclinical settings.

Acknowledgment

The authors would like to thank the anonymous reviewers for their insightful feedbacks.

References

[1] *Sleep Apnea: What Is Sleep Apnea?* NHLBI: Health Inf. Public, U.S. Dept. Health Human Services, Washington, DC, USA, 2010.
[2] P. X. Braun, C. F. Gmachl, and R. A. Dweik, "Bridging the collaborative gap: Realizing the clinical potential of breath analysis for disease diagnosis and monitoring–tutorial," *IEEE Sensors J.*, vol. 12, no. 11, pp. 3258–3270, Nov. 2012.
[3] G. S. Chung *et al.*, "Rem sleep classification with respiration rates," in *Proc. IEEE 6th Int. Special Topic Conf. Inf. Technol. Appl. Biomed. (ITAB)*, Tokyo, Japan, 2007, pp. 194–197.
[4] C. A. Kushida *et al.*, "Practice parameters for the indications for polysomnography and related procedures: An update for 2005," *Sleep*, vol. 28, no. 4, pp. 499–521, 2005.
[5] K.-M. Chen, D. Misra, H. Wang, H.-R. Chuang, and E. Postow, "An x-band microwave life-detection system," *IEEE Trans. Biomed. Eng.*, vol. BME-33, no. 7, pp. 697–701, Jul. 1986.
[6] J. Salmi and A. F. Molisch, "Propagation parameter estimation, modeling and measurements for ultrawideband MIMO radar," *IEEE Trans. Antennas Propag.*, vol. 59, no. 11, pp. 4257–4267, Nov. 2011.
[7] F. Adib, Z. Kabelac, H. Mao, D. Katabi, and R. C. Miller, "Demo: Real-time breath monitoring using wireless signals," in *Proc. MobiCom*, 2014, pp. 261–262.
[8] F. Adib, Z. Kabelac, and D. Katabi, "Multi-person motion tracking via RF body reflections," Comput. Sci. Artif. Intell. Lab., Massachusetts Inst. Technol., Cambridge, MA, USA, Rep. MIT-CSAIL-TR-2014-008, 2014.
[9] N. Patwari, L. Brewer, Q. Tate, O. Kaltiokallio, and M. Bocca, "Breathfinding: A wireless network that monitors and locates breathing in a home," *IEEE J. Sel. Topics Signal Process.*, vol. 8, no. 1, pp. 30–42, Feb. 2014.
[10] O. J. Kaltiokallio, H. Yigitler, R. Jäntti, and N. Patwari, "Non-invasive respiration rate monitoring using a single cots TX-RX pair," in *Proc. IPSN*, Berlin, Germany, 2014, pp. 59–70.
[11] *Fitbit*. Accessed: Dec. 2014. [Online]. Available: http://www.fitbit.com/
[12] *Jawbone Up*. Accessed: Dec. 2014. [Online]. Available: https://jawbone.com/up
[13] *Sleep As Android*. Accessed: Dec. 2014. [Online]. Available: https://sites.google.com/site/sleepasandroid/
[14] T. Hao, G. Xing, and G. Zhou, "isleep: Unobtrusive sleep quality monitoring using smartphones," in *Proc. SenSys*, Rome, Italy, 2013, Art. no. 4.
[15] Y. Ren, C. Wang, J. Yang, and Y. Chen, "Fine-grained sleep monitoring: Hearing your breathing with smartphones," in *Proc. INFOCOM*, 2015, pp. 1194–1202.
[16] R. Nandakumar, S. Gollakota, and N. Watson, "Contactless sleep apnea detection on smartphones," in *Proc. 13th Annu. Int. Conf. Mobile Syst. Appl. Services (ACM Mobisys)*, Florence, Italy, 2015, pp. 45–57.
[17] H. Aly and M. Youssef, "Zephyr: Ubiquitous accurate multi-sensor fusion-based respiratory rate estimation using smartphones," in *Proc. 35th Annu. IEEE Int. Conf. Comput. Commun. (IEEE INFOCOM)*, San Francisco, CA, USA, 2016, pp. 1–9.
[18] *SleepIQ*. Accessed: Dec. 2014. [Online]. Available: http://bamlabs.com/
[19] J. Penne, C. Schaller, J. Hornegger, and T. Kuwert, "Robust real-time 3d respiratory motion detection using time-of-flight cameras," *Int. J. Comput. Assisted Radiol. Surgery*, vol. 3, no. 5, pp. 427–431, 2008.
[20] H. Abdelnasser, K. A. Harras, and M. Youssef, "Ubibreathe: A ubiquitous non-invasive WiFi-based breathing estimator," in *Proc. 16th ACM Int. Symp. Mobile Ad Hoc Netw. Comput.*, Hangzhou, China, 2015, pp. 277–286.
[21] Y. Li, C. Gu, T. Nikoubin, and C. Li, "Wireless radar devices for smart human–computer interaction," in *Proc. IEEE 57th Int. Midwest Symp. Circuits Syst. (MWSCAS)*, College Station, TX, USA, 2014, pp. 65–68.
[22] P. Nguyen, X. Zhang, A. Halbower, and T. Vu, "Continuous and fine-grained breathing volume monitoring from afar using wireless signals," in *Proc. 35th Annu. IEEE Int. Conf. Comput. Commun. (IEEE INFOCOM)*, San Francisco, CA, USA, 2016, pp. 1–9.
[23] B. Fang, N. D. Lane, M. Zhang, A. Boran, and F. Kawsar, "BodyScan: Enabling radio-based sensing on wearable devices for contactless activity and vital sign monitoring," in *Proc. 14th Annu. Int. Conf. Mobile Syst. Appl. Services (ACM Mobisys)*, Singapore, 2016, pp. 97–110.
[24] Y. Wang *et al.*, "E-eyes: Device-free location-oriented activity identification using fine-grained WiFi signatures," in *Proc. MobiCom*, 2014, pp. 617–628.
[25] (2014). *Sleeping Positions to Stay Healthy: The Best and Worst Ways to Sleep During the Night*. [Online]. Available: http://www.medicaldaily.com/sleeping-positions-stay-healthy-best-and-worst-ways-sleep-during-night-296714

[26] J. F. Murray, *The Normal Lung: The Basis for Diagnosis and Treatment of Pulmonary Disease*. Philadelphia, PA, USA: Saunders, 1986.
[27] P. Sebel, M. Stoddart, R. Waldhorn, C. Waldman, and P. Whitfield, *Respiration, the Breath of Life*. New York, NY, USA: Torstar Books, 1985.
[28] *Target Heart Rates—Aha*, Target Heart Rates Amer. Heart Assoc., Dallas, TX, USA, 2014.
[29] L. Davies and U. Gather, "The identification of multiple outliers," *J. Amer. Stat. Assoc.*, vol. 88, no. 423, pp. 782–792, 1993.
[30] R. K. Pearson, "Outliers in process modeling and identification," *IEEE Trans. Control Syst. Technol.*, vol. 10, no. 1, pp. 55–63, Jan. 2002.
[31] *NEULOG Respiration Monitor Logger Sensor*. Accessed: Dec. 2014. [Online]. Available: http://www.neulog.com/
[32] W. Xi *et al.*, "Electronic frog eye: Counting crowd using WiFi," in *Proc. INFOCOM*, Toronto, ON, Canada, 2014, pp. 361–369.
[33] J. T. Bigger *et al.*, "Frequency domain measures of heart period variability and mortality after myocardial infarction," *Circulation*, vol. 85, no. 1, pp. 164–171, 1992.
[34] A. M. Katz, *Physiology of the Heart*. Philadelphia, PA, USA: Lippincott Williams & Wilkins, 2010.
[35] (2003). *Sleep Position Gives Personality Clue*. [Online]. Available: http://news.bbc.co.uk/2/hi/health/3112170.stm
[36] R. O. Duda, P. E. Hart, and D. G. Stork, *Pattern Classification*. Hoboken, NJ, USA: Wiley, 2012.
[37] I. T. Jolliffe, *Principal Component Analysis*. Hoboken, NJ, USA: Wiley, 2002.
[38] D. Halperin, W. Hu, A. Sheth, and D. Wetherall, "Tool release: Gathering 802.11n traces with channel state information," *ACM SIGCOMM Comput. Commun. Rev.*, vol. 41, no. 1, p. 53, 2011.
[39] *Zephyr Technology*. Accessed: Dec. 2014. [Online]. Available: http://zephyranywhere.com/
[40] J. Liu *et al.*, "Tracking vital signs during sleep leveraging off-the-shelf WiFi," in *Proc. 16th ACM Int. Symp. Mobile Ad Hoc Netw. Comput.*, Hangzhou, China, 2015, pp. 267–276.

Jian Liu received the B.E. and M.S. degrees from the Department of Information Engineering, Wuhan University of Technology, Wuhan, China. He is currently pursuing the Ph.D. degree at the Department of Electrical and Computer Engineering, Rutgers University, New Brunswick, NJ, USA.

He was a Research Assistant with the Stevens Institute of Technology, Hoboken, NJ, USA, from 2013 to 2017. He is currently with the Data Analysis and Information Security Laboratory, Rutgers University. His current research interests include cyber security/privacy, mobile computing/sensing, and vehicular systems.

Mr. Liu was a recipient of the Best Paper Award from IEEE SECON 2017.

Yingying (Jennifer) Chen (S'94–M'01–SM'11) is a Professor of electrical and computer engineering with Rutgers University, New Brunswick, NJ, USA, where she is a member of the Wireless Information Network Laboratory and also leads the Data Analysis and Information Security Laboratory. Her background is a combination of physics, computer science, and computer engineering. She was a Tenured Professor with the Stevens Institute of Technology, Hoboken, NJ, USA, and had extensive industry experience with Nokia (formerly Alcatel-Lucent), Boulogne-Billancourt, France. Her current research interests include smart healthcare, cyber security and privacy, Internet of Things, and mobile computing and sensing. She has authored or co-authored over 100 journals and referred conference papers in the above areas.

Dr. Chen was a recipient of the NSF CAREER Award, the Google Faculty Research Award, the NJ Inventors Hall of Fame Innovator Award, the Best Paper Award of IEEE SECON 2017, ACM AsiaCCS 2016, the IEEE CNS 2014, and ACM MobiCom 2011, the IEEE Region 1 Technological Innovation in Academic Award 2017, and the IEEE Outstanding Contribution Award from the IEEE New Jersey Coast Section from 2005 to 2009. Her research has been reported in numerous media outlets, including *MIT Technology Review*, CNN, Fox News Channel, the *Wall Street Journal*, National Public Radio, and *IEEE Spectrum*. She has been serving on the Editorial Boards of the IEEE TRANSACTIONS ON MOBILE COMPUTING and the IEEE TRANSACTIONS ON WIRELESS COMMUNICATIONS.

Yan Wang (GS'12–M'15) received the Ph.D. degree in electrical engineering from the Stevens Institute of Technology, Hoboken, NJ, USA.

He has been an Assistant Professor with the Department of Computer Science, SUNY Binghamton University, Binghamton, NY, USA, since 2015. His current research interests include mobile and pervasive computing, smart healthcare, cyber security and privacy, and wireless networks.

Dr. Wang was a recipient of the Best Paper Award of IEEE SECON 2017 and ACM AsiaCCS 2016, and the ACM MobiCom Student Research Competition in 2013.

Xu Chen received the B.E. degree in electrical engineering from the Stevens Institute of Technology, Hoboken, NJ, USA, in 2016. He is currently pursuing the Ph.D. degree in electrical and computer engineering at Rice University, Houston, TX, USA.

His current research interest includes ubiquitous and pervasive computing.

Jerry Cheng (M'09) received the Ph.D. degree in statistics from Rutgers University, New Brunswick, NJ, USA.

He was a Technical Staff Member with AT&T Laboratories, Florham Park, NJ, USA, and a Post-Doctoral Research Scholar with the Department of Statistics, Columbia University, New York City, NY, USA. He is currently an Assistant Professor with the Robert Wood Johnson Medical School, Rutgers University. His current research interests include data mining and learning, big data analytics, statistical modeling, and statistical applications in engineering and biostatistics.

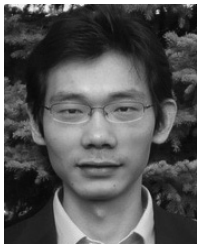

Jie Yang (GS'08–M'12) received the Ph.D. degree in computer engineering from the Stevens Institute of Technology, Hoboken, NJ, USA, in 2011.

He is currently an Assistant Professor with the Department of Computer Science, Florida State University, Tallahassee, FL, USA. His current research interests include cyber security and privacy, and mobile and pervasive computing, with an emphasis on network security, smartphone security and applications, security in cognitive radio and smart grid, location systems, and vehicular applications.

Dr. Yang was a recipient of the Best Paper Award from IEEE CNS 2014 and ACM MobiCom 2011. His research has received wide press coverage, including *MIT Technology Review*, the *Wall Street Journal*, NPR, CNET News, and Yahoo News.